Received: 25 February 2019 | Revised: 4 October 2019 | Accepted: 3 December 2019

DOI: 10.1002/jlcr.3820

RESEARCH ARTICLE

Journal of Labelled Compounds and Radiopharmaceuticals WILEY

Evaluation by metabolic profiling and *in vitro* autoradiography of two promising GnRH-receptor ligands for brain SPECT imaging

Richard Fjellaksel[1,2,3,4] | **Angel Moldes-Anaya**[1,4,5,6] | **Terje Vasskog**[7] | **Ana Oteiza**[1,4] | **Montserrat Martin-Armas**[1,4] | **Ole Kristian Hjelstuen**[1,2] | **Jørn H. Hansen**[3] | **Patrick J. Riss**[8,9,10] | **Rune Sundset**[1,4]

[1]Nuclear Medicine and Radiation Biology Research Group, Department of Clinical Medicine, UiT The Arctic University of Norway, Tromsø, Norway

[2]Drug Transport and Delivery Research Group, Department of Pharmacy, UiT The Arctic University of Norway, Tromsø, Norway

[3]Organic Chemistry Research Group, Department of Chemistry, UiT The Arctic University of Norway, Tromsø, Norway

[4]The PET Imaging Center, University Hospital of North Norway, Tromsø, Norway

[5]Pharmacology Research Group, Department of Pharmacy, UiT The Arctic University of Norway, Tromsø, Norway

[6]Neurobiology Research Group, Department of Clinical Medicine, UiT The Arctic University of Norway, Tromsø, Norway

[7]Natural Products and Medicinal Chemistry Research group, UiT The Arctic University of Norway, Tromsø, Norway

[8]Department of Neuropsychiatry and Psychosomatic Medicine, Oslo University Hospital, Oslo, Norway

[9]Realomics SFI, Department of Chemistry, University of Oslo, Oslo, Norway

[10]Norsk Medisinsk Syklotronsenter AS, Oslo, Norway

Correspondence
Richard Fjellaksel, Nuclear Medicine and Radiation Biology Research Group, Department of Clinical Medicine, UiT The Arctic University of Norway, Tromsø, Norway.
Email: richard.fjellaksel@uit.no

Funding information
Helse Nord RHF, Grant/Award Number: SFP1196-14

The increased expression of gonadotropin releasing hormone receptor (GnRH-R) in brain has been strongly linked to Alzheimer disease. Therefore, the development of radiolabeled imaging agents for GnRH-R is relevant for early diagnosis of Alzheimer disease. We have recently disclosed the discovery of two promising compounds displaying nanomolar-range affinity for the GnRH-R. In the present study, a preclinical evaluation of the compound properties was performed to evaluate their potential as single photon emission computed tomography (SPECT) radiotracers for imaging the GnRH-receptor. The compounds were assessed *in vitro* by performing serum stability analysis by human and rat serum, metabolic profiling by human liver microsomes, and exploratory rat brain autoradiography. The investigated compounds displayed satisfactory stability against human, rat serum, and liver microsomal metabolism, which favors their potential as SPECT-imaging agents. Additionally, we identified and quantified the formation rate of the metabolites by fragmentation of up to

LIST OF ABBREVIATIONS: GNRH, gonadotropin releasing hormone; GNRH-R, gonadotropin releasing hormone receptor; HPG, hypothalamic pituitary gland; HPLC-MS/MS, high performance liquid chromatography mass spectrometry; IHC, immunohistochemistry; LC-MS, liquid chromatography mass spectrometry; LHRH, luteinizing hormone releasing hormone; NADP, nicotinamide adenine dinucleotide phosphate; NADPH, dihydronicotinamide adenine dinucleotide phosphate; SPECT, single photon emission computed tomography.

five mass spectrometric stages. The GnRH-R rat brain specificity of these compounds was tested in competition with a known ligand for the receptor and the *in vitro* autoradiography confirmed that compounds **3** and **4** binds to rat GnRH-R in different rat brain regions.

KEYWORDS

autoradiography, gonadotropin, *in vitro*, metabolic profiling, SPECT

1 | INTRODUCTION

Novel radiotracers are needed to monitor, diagnose and treat diseases, and to develop a deeper understanding of human physiology and pathophysiology.[1,2] Single photon emission computed tomography (SPECT) is a widely used medical imaging technique for diagnosis and monitoring treatments. A SPECT-radionuclide emits a single photon with each disintegration. The photon is further detected by gamma cameras and processed by a computer to generate an image. We have selected to study SPECT as the medical imaging technique due to its major advantages: (a) The technique is less expensive and more convenient compared with other molecular imaging techniques such as positron emission tomography, (b) accessible gamma cameras are available worldwide, and (c) the production of SPECT-radiotracers is not limited to nearby cyclotrons.[3]

Gonadotropin releasing hormone (GnRH) and gonadotropin releasing hormone receptors (GnRH-R) are involved in a wide range of biological processes like reproductive functions, sex behavior, cognition, and more important several diseases such as cancer and neurodegeneration.[4-9] The presence of GnRH-R in the brain is especially interesting since the increase of GnRH-R is strongly linked to Alzheimer disease.[10-16] GnRH-R is mainly expressed in the hypothalamus-pituitary-gonadal axis (HPG axis) together with GnRH where it has its main function in reproductive physiology. The GnRH, also known as luteinizing-hormone releasing hormone (LHRH), is a neurohormone produced in the hypothalamus and released in a pulsatile manner into the hypophysial portal bloodstream. When it reaches the pituitary gland, it binds to its own G-protein coupled receptor (GnRH-R) stimulating the production of two gonadotropic hormones in the anterior pituitary gland—luteinizing hormone and follicle stimulation hormone. Furthermore, the release of gonadotropins acts in the gonads to produce androgens and estrogens. The release of gonadotropins is controlled by the pulsatile release of GnRH in the hypophysial portal blood stream and by the feedback mechanism of androgens and estrogens.[17] Much is yet unknown of the GnRH and GnRH-R involvement in Alzheimer disease. However, dysfunction of the HPG-axis and the feedback mechanism have been shown to be implicated in Alzheimer disease pathophysiology.[10-16]

We have recently revealed the discovery of GnRH-R antagonist candidates based on a benzimidazole-piperazine molecular scaffold suitable for SPECT imaging, compounds **1** and **2**, Figure 1.[18,19] Further diversification

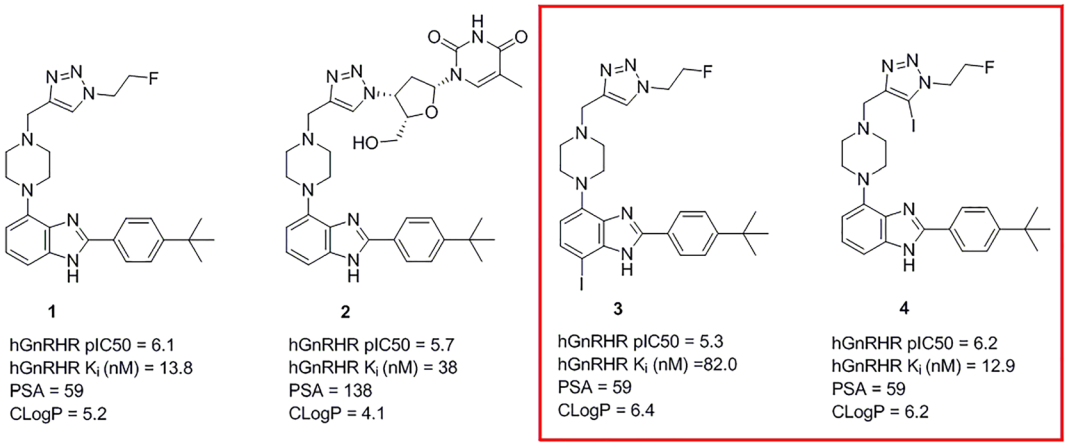

FIGURE 1 Previously disclosed compounds. Compounds **1** and **2** from the initial study.[18] Compounds **3** and **4** were developed in the continuation of the initial study. [20]

from the initial study led to the discovery of two highly promising ^{123}I-labelled triazole-benzimidazole GnRH-R antagonists, compounds **3** and **4**, Figure 1.[20]

In early stage drug development, determination of serum and metabolic stability are essential prior to in vivo evaluation.[21,22] This early stage stability evaluation is especially important in the development of radioiodinated tracers as the rate of metabolism and any possible deiodination process will affect their possible application as a SPECT radiotracer. Furthermore, metabolic profiling is an accurate modeling of metabolic phase I activity enabling us to estimate the metabolism rate and the metabolic deiodination rate which predicts the ability for the drugs as SPECT radiotracers. Therefore, further *in vitro* evaluation of compounds **3** and **4** to develop a SPECT radiotracer targeting the GnRH-R was performed.

Phase I metabolism has also been reported for similar GnRH-R antagonist possessing the same benzimidazole-piperazine scaffold.[23] However, for the radioiodinated analogues included in the present study, a deeper understanding of the rate of metabolism and deiodination was pursued. In the present study serum stability, metabolic profiling from human and rat liver microsomes and rat brain GnRH-R specificity was evaluated by *in vitro* autoradiography to assess the SPECT-imaging potential for these candidates.

2 | EXPERIMENTAL

2.1 | General

Acetonitrile and trifluoroacetic acid were obtained from Sigma Aldrich (St. Louis, Missouri). Silica gel 60 TLC plates with fluorescence indicator (F254) from Merck (Darmstadt, Germany) were used. Anhydrous conditions were conducted only if mentioned. Rat serum and human serum were a kind gift from the Vascular Biology research group at UiT—The Arctic university of Norway. Rat and human liver microsomes were purchased from Thermo Fisher Scientific (Waltham, Missouri) MilliQ water rinsing system from Millipore was used. β-nicotinamide adenine dinucleotide phosphate sodium salt (NADP), β-nicotinamide adenine dinucleotide phosphate reduced tetrasodium salt (NADPH), D-glucose-6-phosphate, and D-glucose-6-phosphate dehydrogenase were also purchased from Sigma Aldrich. ^{125}I-labelled [D-Trp^6]-LHRH was bought from Perkin-Elmer (Norway). Compounds **3** and **4** which were used unlabelled in this study have previously been radiolabelled, and the radiolabelling is described in a previous publication.[20] The synthesis of compounds **3** and **4** are described in section 2.2.

2.1.1 | Animals

Male Wistar Han IGS rats of 6 to 9 weeks of age were purchased from Charles River (Germany). The animals were housed in the Department of Comparative Medicine at UiT—The Artic University of Norway. The animals had access to water and standard chow from Scanbur, BK (Norway) ad libitum. All experimental protocols were approved by The Norwegian Food Safety Authority and conducted in accordance to the Norwegian law, FOR-2017-04-05-451 (Project Fots id: 8353).

2.2 | Synthesis of compounds 3and 4

The key intermediate and compounds **3** and **4** were synthesized according to previous published procedures and details are attached in the supporting information, Scheme 1.[20]

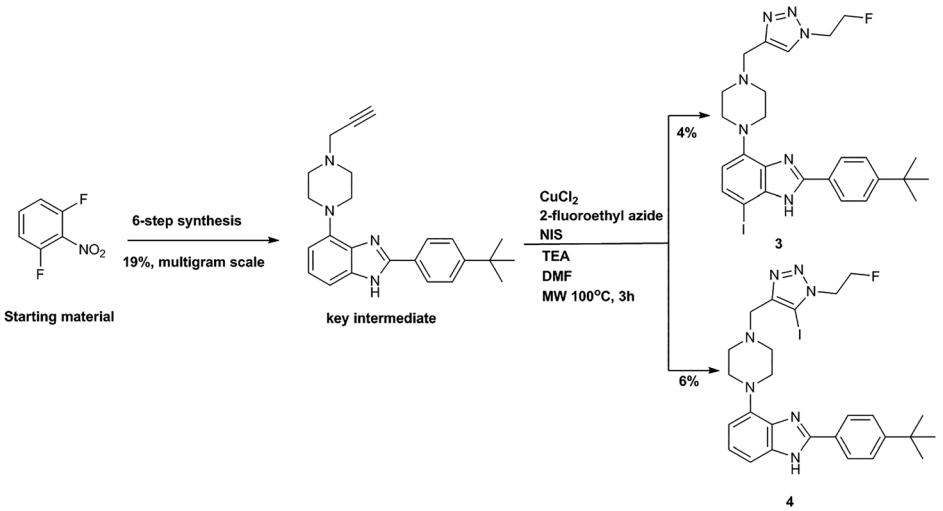

SCHEME 1 Synthetic route for the syntehsis of compounds **3** and **4**

2.2.1 | 2-(4-*tert*-butylphenyl)-4-(4-((1-(2-fluoroethyl)-1*H*-1,2,3-triazol-4-yl)methyl) piperazin-1-yl)-6-iodo-1*H*-benzo[d] imidazole (compound 3)

200 mg (1 Eq, 0.5 mmol) of 2-(4-(*tert*-butyl)phenyl)-4-(4-(prop-2-yn-1-yl)piperazin-1-yl)-1*H*-benzo[d]imidazole **(3)** was added to a solution of 1.7 mL (28 mg/mL) solution of 2-fluoroethyl azide (0.5 mmol, 1 Eq), 76 μL of triethylamine (0.5 mmol, 1 Eq), 100 mg Cu (II)iodide (0.5 mmol, 1 Eq), 135 mg *N*-Iodosuccimide (0.6 mmol, 1.1 Eq) in 10 mL DMF. The reaction mixture heated and stirred by microwave for 3 hours, 100°C. The solvents were evaporated and the compound purified by HPLC. Method: 25 mL/min. initial 95% H_2O 0.1% TFA, 5% ACN 0.1% TFA. At 15 minutes linear change to 5% H_2O 0.1% TFA, 95% ACN 0.1% TFA. The product gave a rf 7.19 minutes, was lyophilized, and gave a white powder. (13 mg, 4% yield). Purity: 95.7 % ^{1}H-NMR (400 MHz, Methanol-d_4), δ in ppm = 8.30(s, 1*H*), 8.10 (d, J = 8.2 Hz, 2*H*), 7.64 (d, J = 8.4 Hz, 3*H*), 6.74 (d, J = 8.3 Hz, 1*H*), 4.81(s, 2*H*), 4.64(s, 2*H*), 3.66 (Br s, 8*H*), 1.41(s, 9*H*) ^{13}C NMR (101 MHz, Methanol-d_4) δ in ppm = 156.2, 141.4, 137.6, 134.8, 129.0, 128.7, 127.1, 113.9, 83.6 ($^1J^{CF}$ = 170 Hz), 81.9 ($^1J^{CF}$ = 170 Hz), 52.8, 52.2 ($^2J^{CF}$ = 20 Hz), 52.0 ($^2J^{CF}$ = 20 Hz), 51.7, 35.9, 31.6 IR (neat): 2966, 1664, 1460, 1182, 1132 HRMS ESI m/z: Found 588.1743 $[M+H]^+$ Calculated 588.1748.

2.2.2 | 2-(4-*tert*-butylphenyl)-4-(4-((1-(2-fluoroethyl)-5-iodo-1*H*-1,2,3-triazol-4-yl) methyl)piperazin-1-yl)-1*H*-benzo[d] imidazole (compound 4)

200 mg (1 Eq, 0.5 mmol) of 2-(4-(*tert*-butyl)phenyl)-4-(4-(prop-2-yn-1-yl)piperazin-1-yl)-1*H*-benzo[d]imidazole **(3)** was added to a solution of 1.7 mL (28 mg/mL) solution of 2-fluoroethyl azide (0.5 mmol, 1 Eq), 76 μL of triethylamine (0.5 mmol, 1 Eq), 100 mg Cu (II) iodide (0.5 mmol, 1 Eq), 135 mg *N*-Iodosuccimide (0.6 mmol, 1.1 Eq) in 10 mL DMF. The reaction mixture heated and stirred by microwave for 3 hours, 100°C. The solvents were then evaporated and purified by HPLC. Method: 25 mL/min. initial 95% H_2O 0.1% TFA, 5% ACN 0.1% TFA. At 15 minutes linear change to 5% H_2O 0.1% TFA, 95% ACN 0.1% TFA. The product gave a rf 7.19 minutes, was lyophilized, and gave a white powder (19 mg, 6% yield). Purity = 95.9% ^{1}H-NMR (400 MHz, methanol-d_4), δ in ppm = 8.08 (d, J = 8.1 Hz, 2*H*), 7.72 (d, J = 7.6 Hz, 2*H*), 7.46 (d, J = 4.9 Hz, 2*H*), 7.13(s, 1*H*), 4.59(s, 2*H*), 3.72(Br s, 8*H*), 1.39(s, 9*H*) ^{13}C NMR (101 MHz, Methanol-d_4) δ in ppm = 157.5, 151.9, 142.7, 140.9, 136.0, 131.3, 128.8, 127.6, 127.0, 124.1, 114.1, 109.7, 89.0, 83.4($^1J^{CF}$ = 171 Hz), 81.7($^1J^{CF}$ = 171 Hz), 53.1, 52.7($^2J^{CF}$ = 20 Hz), 52.5($^2J^{CF}$ = 20 Hz), 52.3, 36.1, 31.5 IR (neat): 2965, 1663, 1437, 1179, 1126 HRMS ESI m/z: Found 588.1743 $[M+H]^+$ Calculated 588.1748.

2.3 | Evaluation of compounds 3 and 4 in human and rat serum

The stability of compounds **3** and **4** was investigated in human and rat serum. In assay, compounds **3** and **4** were dissolved in a mixture of ethanol/polysorbate 80/water for injection (5:5:90). The compounds were then incubated with 400 μL human and 300 μL rat serum, to give a final concentration of 5mM and 6.5mM at 37°C, respectively. An aliquot (40-50 μl) was subsequently extracted with ice-cold acetonitrile at 0, 10, 30, 60, 120, 240, and 1320 minutes post-incubation. Samples were centrifuged at 13000*g* for 5 minutes. The supernatants were collected and analyzed by LTQ Orbitrap XL with electrospray ion source (ION-MAX) and thermo scientific Accela autosampler with Thermo Hypersil Gold 50 × 2.1 mm, 1.9 um C18 reverse phase column. The detection window was constrained to m/z 400 to 620 and the percentage remaining compound left in the samples were analyzed. Instrument characteristics and program parameters for serum stability analysis are provided in the Supporting Information.

2.4 | Incubation with rat and human liver microsomes

In brief, stock solutions (2mM) of the substrates were prepared by dissolving compounds **3** and **4** in acetonitrile: water (v/v, 75:25). The compounds were incubated in a total volume of 1 mL in Pyrex test tubes at 37°C in a shaking water bath (Heto-Holten, Allerod, Denmark) with rat and human liver microsomes. Human liver microsomes consisted on a mixed gender pool of 15 donors (20 mg/mL protein), whereas rat liver microsomes consisted of an undetermined number of male donors at 20 mg/mL protein. The incubation was performed in NADPH regeneration system in HEPES buffer (pH 7.4) containing 19.4mM glucose-6-phosphate, 0.91mM NADPH, 0.84mM NADP, and 5.72 units of glucose-6-phosphate dehydrogenase.[24] At 0, 2, 5, 15, 30, 60, 120, and 180 minutes, 0.1 mL aliquots were taken and transferred to Eppendorf tubes containing 0.1 mL ice-cold acetonitrile and 100 ng/mL internal standard to quench the reaction. The samples were centrifuged at 21000*g* in a 5424R Eppendorf centrifuge (VWR, Oslo, Norway). The

supernatants were then collected and transferred to HPLC insert-vials for further analysis on the LC-MS system. Positive and negative controls were included in each incubation mixture in order to validate the experimental setup. As a positive control, lidocaine was used, the metabolism of lidocaine is shown in Figure S3. Lidocaine has a well-known metabolic profile and, in addition, structural similarities with the substrates to be studied in the present study.[25,26] As negative control, a mixture containing all the components of the experiments except the substrates and an incubation containing the substrates without the microsomes was included.

2.5 | Semi-quantitative analysis of compounds 3and 4 and screening for metabolites

The assumption of similar response for the metabolites as for the parents is unrealistic, and the concentrations should therefore clearly be regarded as semi-quantitative. However, the relative concentrations of each metabolite over time illustrate the metabolization in a representative manner. 2-(4-(*tert*-butylphenyl)-4-(4-(2-fluoroethyl)piperazin-1-yl)-1*H*-benzo[d]imidazole was used as an internal standard at a concentration of 100 μg/mL. Calibration curves were constructed for the parent compounds (**3** and **4**) in a concentration range from 0.5 to 8 μg/mL. Calibration standards were made in matrix and showed appropriate linearity in the range of the concentrations studied, experiments were performed at least three times, with at least three injections each time. The linearity for compound **3** was found to be $R^2 = 0.9731$, y = 0.1929x + 0.1354, for compound **4** $R^2 = 0.9608$, y = 0.2072x + 0.1426.

2.6 | HPLC-MS/MS

The rate of metabolism and metabolite identification was performed on a Waters (Millford, Massachusetts) Xevo G2 Q-ToF mass spectrometer connected to a Waters Acquity UPLC I-class separation module. The separation was achieved on a Waters Acquity BEH C18 2.1 × 100 mm column with 1.7 μm particle size. The mobile phases consisted of A: water with 0.1% formic acid and B: acetonitrile with 0.1% formic acid. The analysis was performed with gradient elution starting with 2% B with a linear increase to 95% B after 10 minutes. The flow rate was set to 0.6 mL/min, the injection volume was 5 μL, and the column temperature was set to 65°C. For full scan analysis of all compounds, the mass spectrometer had a capillary voltage of 600 V, the cone voltage was set to 30 V, the cone gas flow was set to 10 L/h and 130°C, and the desolvation gas flow was set to 800 L/h and 450°C. Nitrogen from a Genius NM32LA nitrogen generator (Peak Scientific, Incinnan, Great Britain) was used as both cone and desolvation gas. The mass range was set to m/z 105 to m/z 1200, and the analysis was performed with positive electrospray ionization. Leucine-enkephaline with an m/z of 556.2771 was used as lockspray for increased mass accuracy. For MS/MS experiments, similar settings were used but instead of full scan analysis the protonated molecular ion of each compound was set as precursor ion for fragmentation. The fragmentation was done by collision induced fragmentation with argon (Aga, Oslo, Norway) as collision gas, and a collision energy ramp of 20 to 40 eV was used for all compounds. Fragments were detected in the mass range m/z 50 to m/z 650. Identification of metabolites was done manually by considering normal phase 1 metabolism and by the software Metabolynx by Waters set to identification of phase 1 metabolites.

2.7 | HPLC-MS/MS for characterization of metabolites

To obtain as much structural information about the metabolites as possible a Thermo Scientific LTQ Orbitrap XL with electrospray ion source (ION-MAX) was used with fragmentation up to MS^5. Additional fragmentation spectra and program parameters are given in the supporting information. The interpretation of MS^n spectra is not confirmed by isotopic labelling of the compounds and is based on theoretical fragmentation patterns from the software Metabolynx which is part of the Waters Masslynx software, as well as experiential knowledge. This means there might be an uncertainty in some of the structures with regard to the position of functional groups, etc.

2.8 | Preliminary rat brain autoradiography studies

Rats were anesthetized using isoflurane (Induction 4%, maintenance 2% in oxygen) and euthanized while still under anesthesia with an overdose of pentobarbital (100 mL/kg) administered intraperitoneally. Brains were rapidly removed, embedded in O.C.T. Tissuetek (Sakura-Finetek, USA) and frozen by immersion in isopentane and liquid nitrogen. Coronal brain sections (−20°C, 20 μm thickness) were prepared on a cryostat and mounted on Superfrost Plus glass slides (Carl Roth GmbH & Co KG, Karlsruhe, Germany). Sections were

allowed to thaw and dry at room temperature for 30 minutes. Samples were pre-incubated with TMSA buffer (25mM Tris, 5mM $MgCl_2$, 32mM sucrose, 1% BSA, pH 7.4) for 30 minutes. Thereafter, incubation with compounds **3** and **4** in different concentrations, ranging from 0 to 100mM for 60minutes, was performed at room temperature in TMSA buffer. Slides were washed with TMSA buffer for 5 minutes and incubated for 60 minutes at room temperature with ^{125}I-labelled [D-Trp6]-LHRH (0.1 nM). The sections were then washed four times with ice cold TA buffer (25mM Tris, 1% BSA pH 7.4) and once in milliQ water for 5 minutes. The samples were dried, exposed to a phosphor imaging screen (FUJI BAS-MS 2340 GE Healthcare Lifescience) for 7 days at −20°C, and scanned with Fujifilm bio-imaging analyser BAS-5000. Images were processed by Image J software (NIH). For the morphological studies, the slides were kept at −80 and later labelled with fresh SignalStain DAB Substrate (CST #8059) taking advantage of the intrinsic peroxidase catalytic activity of the tissue. Rat brain histological pictures were taken with a VS120 Virtual Slide Microscope (Olympus) with a x20 magnification.

3 | RESULT AND DISCUSSION

Compounds **3** and **4** were synthesized in a seven-step synthesis as shown in the experimental section with a non-optimized yield of 4% for **3** and 6% for **4**, Scheme 1. Serum stability of compounds **3** and **4** was studied by LC-MS, and results are shown in Table 1. The compounds were found to be stable *in vitro* in both human and rat serum. A minimum of 81% of the compounds remained after 120 minutes incubation. After 22 hours, more than 70% of the compounds remained, indicating good stability in human and rat serum.

The next step in the radiotracer development of compounds **3** and **4** required metabolic profiling to investigate their stability for phase 1 metabolism. MS/MS fragment ions of compounds **3** and **4** were identified by LC-MS/MS and are shown in Figure 2. The identity of

TABLE 1 Serum stability of compounds 3 and 4 in human and rat serum

	Compound 3	Compound 4	Compound 3	Compound 4
Minutes	Human serum[a]	Human serum[a]	Rat serum[a]	Rat serum[a]
0	100	100	100	100
30	97	109	101	98
60	107	99	94	92
120	103	106	98	81
1320	84	91	86	70

[a]Stability given as the mean of two experiments.

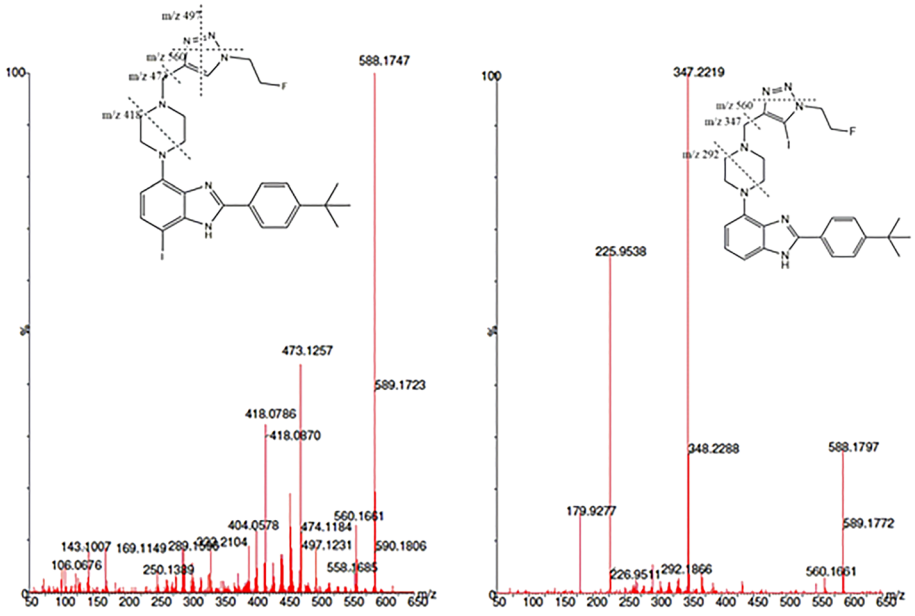

FIGURE 2 Structural information obtained by LC-MS/MS. MS/MS spectrum of compound **3** to the left and compound **4** to the right. Major product ions are shown in the structures as mass to charge ratio (m/z)

TABLE 2 Compound **3** incubated with human liver microsomes

Identity	Retention Time, minutes	$[M+H]^+$	Metabolite Description	Major Fragment Ions (*m/z*)
3	4.01	588	Parent	560, 497, **473,** 418,
M1	3.05	604	3 [+OH]	576, **489,** 434
M2	2.91	578	3 [$+H_2O$, $-CH_3$, $-CH_3$]	461, 434, 307, **295**
M3	3.82	584	3 [two sequential desaturations]	a
M4	3.79	461	3 [$-C_5H_6N_3F$]	a
M5	2.82	477	3 [$+OH-C_5H_6N_3F$]	a

Note. Structural information obtained by LC-MS and LC-MS/MS of metabolites. Bold values represent diagnostic fragment ions.
[a]Unable to obtain reliable MS/MS data due to very low ion signals.

TABLE 3 Compound **4** incubated with human liver microsomes

Identity	Retention Time, minutes	$[M+H]^+$	Metabolite Description	Major Fragment Ions (*m/z*)[a]
4	3.17	588	Parent	560, **347,** 292, 226, 180
M1	2.26	604	4 [+OH]	**363**, 308, 226, 180
M2	1.98	478	4 [+OH-I+H]	363, **308**,
M3	2.52	335	4 [$-C_5H_5N_3FI$]	**292**, 277, 262,
M4	2.16	558	4 [$+OH-C_2H_3F$]	**402**, 351, 308, 277
M5	2.08	578	4 [$+H_2O-CH_2-CH_2$]	**337**, 308, 226, 180
M6	3.07	542	4 [$-C_2H_3F$]	386, **335**, 292, 278, 266

[a]*Note.* Structural information obtained by LC-MS and LC-MS/MS of metabolites in human microsomes. Bold values represent diagnostic fragment ions.

the produced metabolites was achieved based on the comparison of fragmentations for the metabolites and the parent compounds, and the structures were partly determined. MS^n spectra with structural information of metabolites can be found in Figures S4 to S39. An overview of molecular ions and main fragment ions of the metabolites are given in Tables 2 and 3.

Major fragment ions for compound **3** were identified as *m/z* 560, 497, 473, 418, 333, and 292. The fragment ion *m/z* 560 is due to a loss of two nitrogen atoms, from the triazole-ring. The *m/z* 497 fragment is due to a fragmentation of the triazole-ring where the fluoroethyl group in addition is lost, while the fragment *m/z* 473 is due to the loss of the entire triazole-ring including the fluoroethyl group. Signal m/z 418 is due to a fragmentation of the piperazine ring.

The metabolites from compound **3** were identified as M1 *m/z* 604 (hydroxylation), M2 *m/z* 578 (hydration and two demethylations), M3 *m/z* 584 (two sequential desaturations), M4 *m/z* 461 (loss of the fluoroethyl-group), and M5 *m/z* 477 (hydroxylation and loss of the fluoroethyl-group) as shown in Table 2.

M1 (*m/z* 604) shows a typical difference of 16 amu compared to compound **3** at *m/z* 588, which is due to a hydroxylation product. The MS/MS spectrum shows a fragment ion at *m/z* 576, equal to fragment *m/z* 560 of compound **3**. The signal at *m/z* 489 and *m/z* 434 is equal to the signal at *m/z* 473 and *m/z* 418 of compound **3**. M2 (*m/z* 578) is 10 amu lower than for compound **3** at *m/z* 588, due to hydration and two demethylations. The fragment ions at *m/z* 461 and *m/z* and 434 are equal to *m/z* 473 and *m/z* 418 for compound **3**. The signal *m/z* 307 is equal to *m/z* 418 for compound **3** but with an additional loss of iodine on the benzimidazole. The signal at *m/z* 295 is equal to the fragment *m/z* 418 for compound **3**, however due to the additional loss iodine and 12 amu, which reflects the loss of a carbon nearby the nitrogen in the piperazine ring. Identification of the metabolites M3, M4, and M5 was performed by LC-MS and MS/MS analysis of the parent and fragment ions and additionally by the Metabolynx toolbox from MassLynx software (Waters).

There is a remarkable similarity between metabolism by rat and human liver microsomes for compound **3**, as shown in Figure 3. Notably, compound **3** is metabolized at a slightly slower rate in human liver microsomes compared with rat liver microsomes. The maximum amount of M1 is produced within 15 to 30 minutes. In addition, M1 and M2 are produced at a lower rate in human than in rat liver microsomes. Additionally, the half-life of compound **3** incubated in human liver microsomes was found to be 43 minutes and for rat liver microsomes 47 minutes.

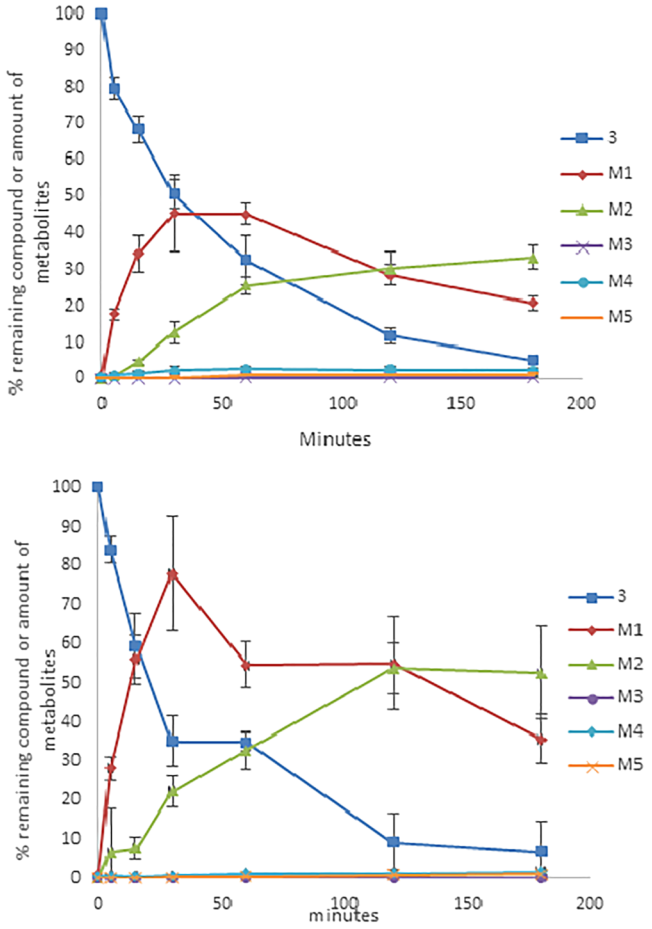

FIGURE 3 Metabolic transformation of compound **3** with metabolites. Upper graph presents the compound incubated with human liver microsomes and the lower graph with rat liver microsomes. The experiment was performed as two independent experiments with four injections on LC MS-MS

The metabolites M3 to M5 were produced in minor amounts (Figure 3).

The ion chromatograms for compound **3** and the metabolites M1 to M5 are shown in Figure S1, where the increase of the metabolites is seen at the selected time points 15 and 180 minutes for compound **3**.

For compound **4,** the fragmentation by LC-MS/MS revealed the major fragment ions as *m/z* 560, 347, 292, 226, and 180. Similarly as for compound **3,** the loss of two nitrogen atoms is due to the fragment signal of *m/z* 560 from compound 4. The *m/z* 347 fragment ion is due to a loss of triazole with the fluoroethyl group in addition to the loss of iodine. The signal *m/z* 292 is due to a cleavage of the piperazine ring. The *m/z* of 226 and m/z 180 are due to a fragmentation in the triazole, where the signal at m/z 226 indicates that the fluoroethyl group is still present.

The metabolites from compound **4** were identified as M1 *m/z* 604 (hydroxylation), M2 *m/z* 478 (hydroxylation and deiodination), M3 *m/z* 335 (loss of the triazole with the fluoroethyl group and iodine), M4 *m/z* 558 (hydroxylation and loss of the fluoroethyl group), M5 m/z 578 (hydration and demethylation), see Table 3. M1 (m/z 604) shows a difference of 16 amu compared with compound **4**, which is due to a hydroxylation product. Furthermore, fragment ions of M1 (*m/z* 604) corresponds to a large degree on the fragments of compound **4** (fragment *m/z* 363 corresponds to *m/z* 347, fragment *m/z* 308 corresponds to *m/z* 292, fragment *m/z* 226 corresponds to *m/z* 226, and fragment *m/z* 180 corresponds to *m/z* 180). M2 (*m/z* 478) is due to a hydroxylation in addition to a deiodination. The fragment ions of M2 corresponds to a large degree on the fragments of compound **4** (fragment *m/z* 363 corresponds to *m/z* 347, fragment *m/z* 308 corresponds to *m/z* 292). In addition, signals *m/z* 226 and *m/z* 180 are missing, which makes iodine on the triazole important for the fragmentation, and when the iodine is missing, these fragments are also missing. M3 (*m/z* 335) is due to the loss of the triazole with the fluoroethyl group and the iodine. The fragment ions for M3 also correspond to a large degree to the fragments for compound **4** (fragment *m/z* 292 corresponds to *m/z* 292, fragment *m/z* 277, and *m/z* 262 corresponds to *m/z* 292). Fragment ion *m/z* 292 is due to the loss of one CH_2-group and subsequently another CH_2-group. In addition, the signals *m/z* 226 and *m/z* 180 are missing here as well, again indicating the importance of the iodine on the triazole for the fragmentation. M4 (*m/z* 558) is due to a hydroxylation with the loss of the fluoroethyl group at the triazole. Additionally, the fragment ions for M4 (*m/z* 558) corresponds to a large degree on the fragments for compound **4** (Fragment *m/z* 402 corresponds to *m/z* 560 for compound **4** with the additional loss of iodine, fragment *m/z* 351 corresponds to *m/z* 347, however with the additional loss of a carbon, *m/z* 308 corresponds to *m/z* 292, fragment *m/z* 277 corresponds to *m/z* 292, due to the loss of one CH_2-group). The signal for M5 (*m/z* 578) is due to a hydration and two demethylations. As for the other metabolites the fragment ions for M5 (*m/z* 578) corresponds to a large degree to the fragment ions for compound 4 (signal *m/z* 337 corresponds *m/z* 347, *m/z* 308 corresponds to *m/z* 292, *m/z* 226 corresponds to *m/z* 226, and *m/z* 180 corresponds to *m/z* 180). M6 (*m/z* 542) is due to a fragmentation of the fluoroethyl group. The fragment ions for this metabolite also correspond to a large degree to the fragment ions for compound **4** (The *m/z* 386 is due to the loss of iodine and two nitrogen atoms). The *m/z* 335 corresponds to *m/z* 347 with the additional loss of a carbon, signal *m/z* 292 corresponds to *m/z* 292. The *m/z* 278 and *m/z* 266 corresponds to *m/z* 292 (difference of 12 amu) is due to a

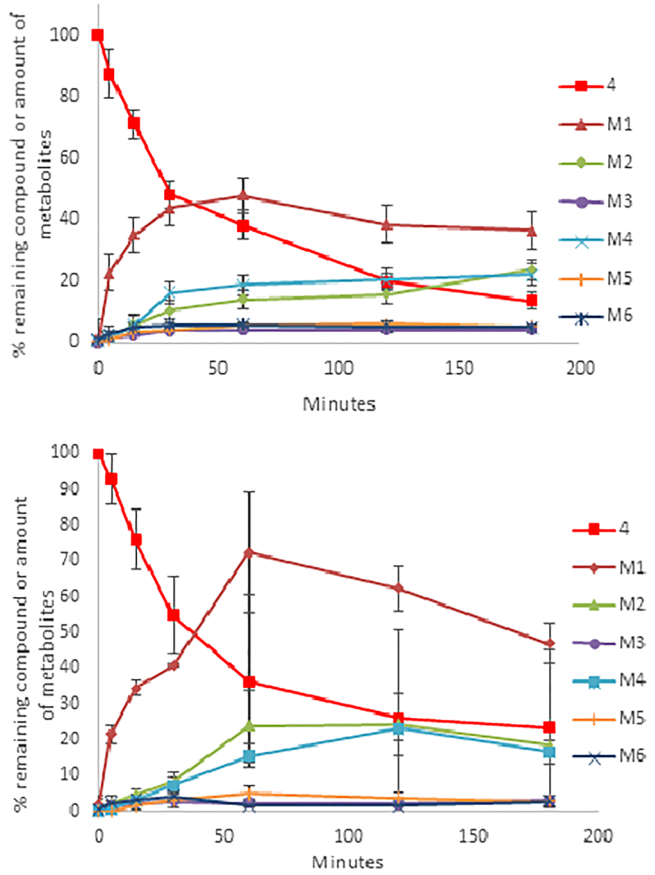

FIGURE 4 Metabolic transformation of compound **4** with metabolites. Upper graph presents the compound incubated with human liver microsomes and the lower graph with rat liver microsomes. The experiment was performed as two independent experiments with four injections on LC MS-MS

fragmentation on the piperazine where only a nitrogen is left for *m/z* 266).

As with compound **3**, the metabolism of compound **4** is similar in human and rat liver microsomes. However, in the case of compound **4,** the metabolism in rat liver microsomes appears to be slightly slower than in human liver microsomes**,** Figure 4. The main found metabolites are M1, M2, and M4. More M1 are formed as compared to M2 and M4 in human and rat liver microsomes. The minor metabolites were M3, M5, and M6. Additionally, the half-life for compound **4** incubated in human liver microsomes was found to be 64 minutes and for rat liver microsomes 86 minutes.

The ion chromatograms for compound **4** and the metabolites M1-M6 are shown in Figure S2, where the time-dependent increase in the metabolite levels are also shown at the selected time points 15 and 180 minutes, respectively.

Structural studies were performed in some of the major metabolites. To identify the most probable position for the hydration of metabolite M2 (compound **3**) and the hydroxylation on the metabolite M1 (compound **3**) and the metabolites M1, M2, and M4 (compound **4**), further MS^n experiments were performed. Metabolite M2 for compound **3** show two demethylations with a sequential hydration. The most probable place such a demethylation will occur is at the *tert*-butyl group. Fragmentation of M2 (compound **3**) by MS^2 to MS^5 where performed and several fragment ions were identified, Figure 5 (MS^2). Additionally, fragment ions for compound **3** where analyzed by MS^2 to MS^5 and compared with M1 (MS^2 and MS^3) and M2 (additional spectra in the Supporting Information).

Furthermore, compound **4** was analyzed by MS^2 to MS^5 for fragmentation patterns. Metabolite M2 was fragmented to MS^5 to identify the fragment ion for M2 from compound **4**. The fragment ions *m/z* 132.2 and 116.2 indicate that the hydroxylation occurred at the benzene-ring on the benzimidazole group in Figure 6. For the metabolites M1 (MS^2 to MS^5) and M4 (MS^2 and MS^3), the same fragmentation patterns are seen as for M2 (compound **4)** for MS^2 to MS^5 which indicates that the hydroxylation occur at the same position for these metabolites. Additionally, the same fragmentation pattern was observed for metabolite M1 (compound **3)** in MS^2 and MS^3 spectra as for metabolites M1, M2, and M4 (compound **4**) indicating the hydroxylation occurs at the benzene-ring on the benzimidazole.

The metabolic profile identified five metabolites for compound **3** and six metabolites for compound **4**. In light of the serum stability analysis and the metabolic profiles, the metabolism of compounds **3** and **4** both in rat- and human-liver microsomes is acceptable for an imaging agent in human and rat. The metabolic half-life was found to be 43 minutes (human liver microsomes) and 47 minutes (rat liver microsomes) for compound **3**. The half-life for compound **4** incubated in human liver microsomes was found to be 64 minutes and for rat liver microsomes 86 minutes. Even though the half-life for compound **4** is relatively longer than compound **3**. The half-lives indicate that compounds **3** and **4** may be suitable as SPECT-imaging agents. The metabolic profile for both compounds **3** and **4** are suitable for imaging agents and the rates of metabolism and deiodination make them highly interesting for further evaluation.

The serum stability analysis, metabolic profiling, binding potential, and the lipophilicities according to PSA and CLogP (Figure 1) lead us to further examine compounds **3** and **4** as possible brain SPECT radiotracers. For preliminary evaluation, the binding potential of these compounds to rat brain GnRH-R was assessed by *in vitro* rat brain autoradiography. Compounds **3** and **4** were

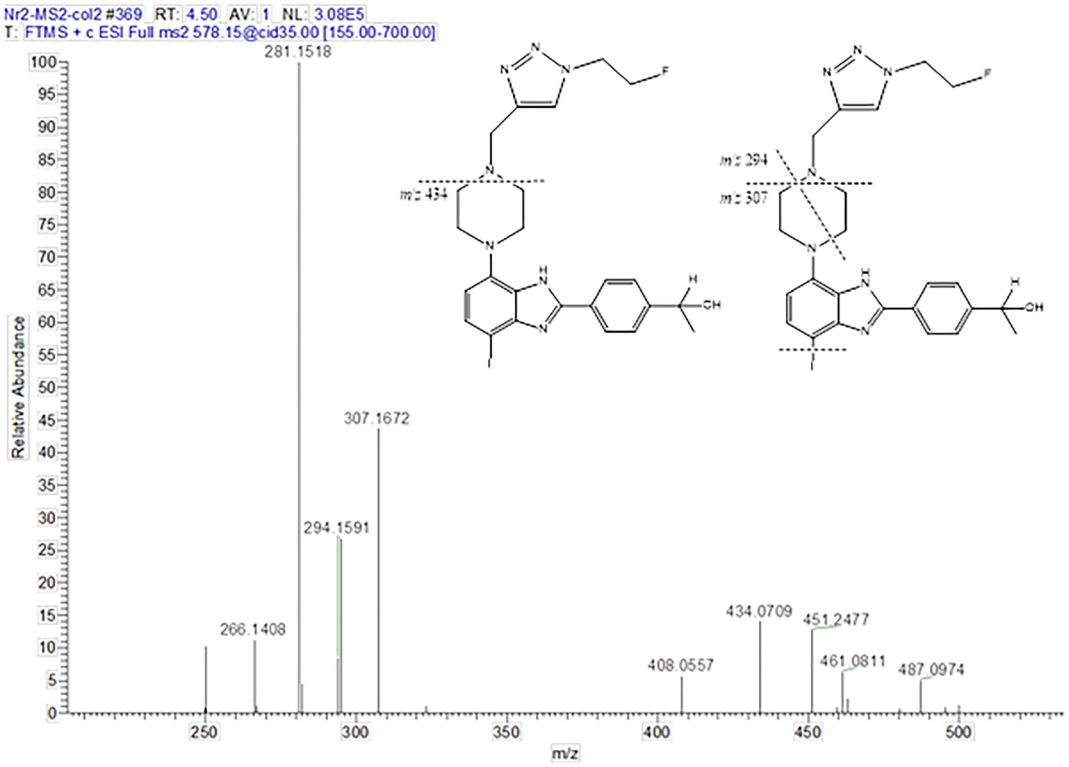

FIGURE 5 MS^2 spectra for fragment ions for the metabolite M2 (compound **3**) which most likely identifies M2 which occurs by two demethylation with a sequential hydration

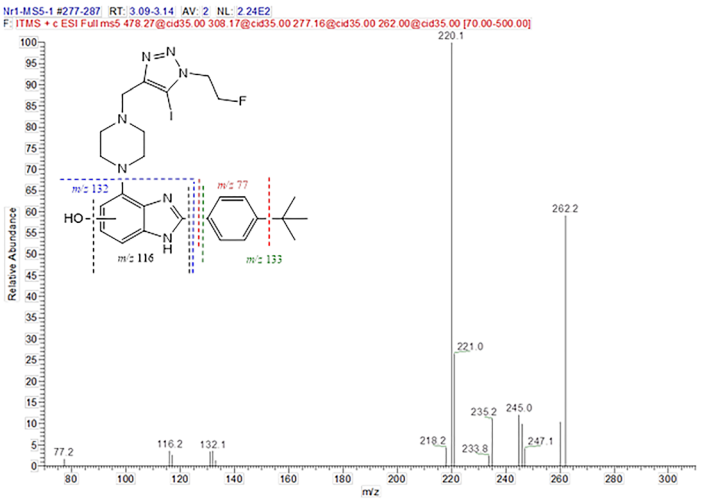

FIGURE 6 MS^5 spectra to identify the fragment ions for hydroxylation on metabolite M2 for compound **4**

incubated in a competitive binding against the GnRH-R agonist [^{125}I]-[D-Trp6]-LHRH.

The identifications of the different brain areas whereas the competition for the receptor can be observed were achieved by the observation and subsequent comparison of the *in vitro* autoradiography data, DAB stained histological sections and the Rat Brain Atlas 4.0[27] (Figure 7). The decrease in the signal shows that compounds **3** and **4** specifically displace the radiolabeled GnRH agonist [^{125}I]-[D-Trp6]-LHRH. Compound **3** shows high binding in areas of the corpus callosum, striatum, and specially the optic nerve area. For compound **4**, autoradiographic data shows intense binding in areas of the hippocampal formation, cortex, and the midbrain regions.

In a previous study by Jennes et al,[28] most pronounced uptake of a GnRH agonist in the rat brain was observed in the hippocampal formation. In line with these observations, our data for compound **4** (Figure 7) show high specific binding in the hippocampal areas. Additionally, and also matching the observations of Jennes et al, higher uptake was observed in the subiculum and the midbrain regions. Furthermore, Skinner

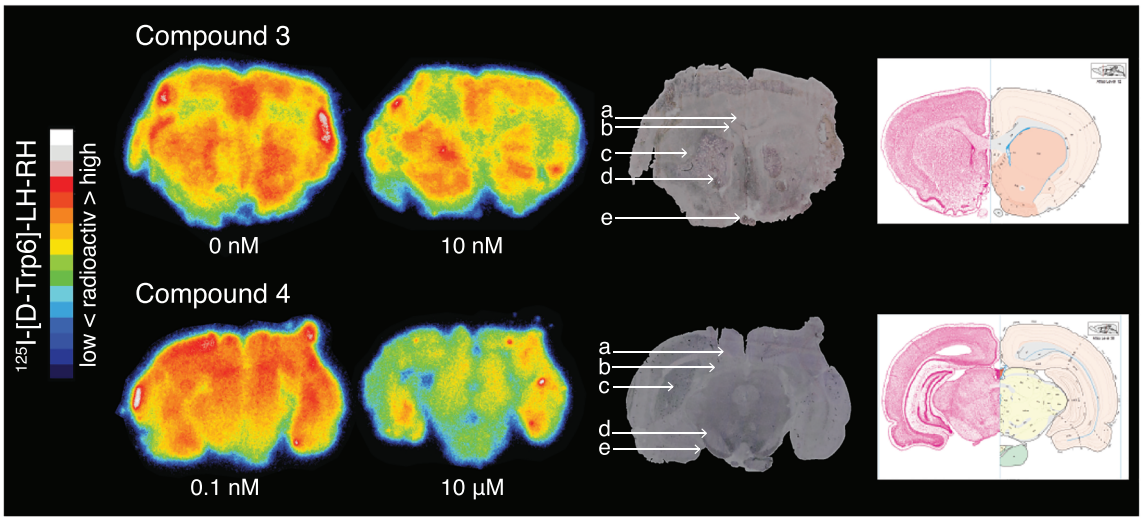

FIGURE 7 Representative brain autoradiography showing the competition of compounds **3** and **4** against ^{125}I[D-Trp6]-LH-RH at two concentration levels, n = 3. The autoradiographic pictures were compared against histological DAB-staining and Rat Brain Atlas 4.0 on right side. For compound **3**, 0 nM was selected as basal ^{125}I[D-Trp6]-LH-RH binding and 10 nM for displacement. For compound **4**, 0.1 nM was selected as basal ^{125}I[D-Trp6]-LH-RH binding and 10 µM was selected due to displacement of the radioligand. Identified areas for compound **3**, (a) genu of corpus callosum, (b) anterior horn of lateral ventricle, (c) striatum, (d) olfactory limb of anterior commissure, (e) optical nerve. For compound **4**, (a) subiculum, (b) ventricle, (c) hippocampal area, (d) substantia nigra, (e) hippocampal fissure

et al,[9] identifies GnRH effects and GnRH receptors outside the hypothalamo-pituitary-gonadal axis. Our results for compound **3** are in accordance with the described areas in Skinner publication showing high specific uptake in cortex and striatum (Figure 7). Additionally, immunohistochemistry (IHC) experiments were performed using GnRH antibody. However, in our attempts to identify the GnRH receptors by immunohistochemistry, after the AR protocol, no co-localization between primary antibody and ^{125}I-labelled [D-Trp6]-LHRH was found. The results are not conclusive since multiple factors are known to affect IHC protocols, most curious is that our IHC pictures corresponds to those shown by Jennes et al.[28]

Compound **4** showed a stronger reduction of the [^{125}I] [D-Trp6]-LHRH binding to GnRH-R compared with compound **3**. At a displacing concentration of 10µM, compound **4** is able to almost completely inhibit the binding of [^{125}I] [D-Trp6]-LHRH with an Ki 0.3 nM[29] for GnRH-R in the rat brain. This is in consistency with our previous findings showing that the inhibition potency of compound **4** (K_i of 12.9 nM) was six-fold higher that of compound **3** (K_i of 82 nM).[20]

4 | CONCLUSIONS

Compounds **3** and **4** were evaluated *in vitro* to determine crucial properties concerning to their suitabilities as GnRH-R molecular imaging agents. More than 70 % of the compounds remained in rat- and human- serum for 22 hours, which indicates that the compounds were quite stable in rat and human serum. A thorough analysis of the phase 1 metabolism for compounds **3** and **4** revealed a metabolic half-life suitable for the possible application of these compounds as SPECT imaging agents. Five metabolites were identified and semi-quantified for compound **3** and six metabolites were identified and semi-quantified for compound **4**. Additionally, *in vitro* autoradiography confirmed the binding potential of compounds **3** and **4** to rat GnRH-R in different rat brain regions in competition to the agonist [^{125}I] [D-Trp^6]-LHRH. In conclusion, a more suitable metabolic profile and affinity for the GnRH receptor favorizes compound **4** as the most promising SPECT radiotracer. Further, in vivo characterization of these promising compounds as GnRH-R SPECT radiotracers will be explored.

ACKNOWLEDGEMENTS

The authors greatly acknowledge Helse Nord RHF for funding this project and the assistance from engineer Jostein A. Johansen for the in depth MS analyses.

ETHICS APPROVAL AND CONSENT TO PARTICIPATE

The study does not involve human participants, human data, or human tissue. Animals were used in this study,

and ethical approval was given as all experimental protocols were approved by The Norwegian Food Safety Authority and conducted in accordance to the Norwegian law, FOR-2017-04-05-451 (Project Fots id: 8353).

AVAILABILITY OF DATA AND MATERIAL

All data generated or analyzed during this study are included in this published article and in the supplementary information file.

COMPETING INTEREST

The authors declare no conflict of interest.

FUNDING INFORMATION

The authors gratefully acknowledge funding for this project from Northern Norway Regional Health Authority (Helse Nord RHF) [SFP1196-14].

AUTHOR CONTRIBUTIONS

R.F., A.M.A., T.V., A.O., and M.M.A. are responsible for the study design. R.F. performed the synthetic work. The serum stability assay was performed by R.F. The metabolic study was performed by A.M.A. and R.F. Analysis of the metabolic data was performed by T.V., A.M.A., and R.F. The autoradiography studies were performed by A.O., M.M.A., and R.F. based on a protocol from P.J.R. Analysis of data was performed by all authors. Major contribution in manuscript preparation R.F., with input from all other authors.

ORCID

Richard Fjellaksel https://orcid.org/0000-0002-6783-5198
Patrick J. Riss https://orcid.org/0000-0002-3887-7065

REFERENCES

1. Evans NR, Tarkin JM, Buscombe JR, Markus HS, Rudd JHF, Warburton EA. PET imaging of the neurovascular interface in cerebrovascular disease. *Nat Rev Neurol*. 2017;13:676-688.
2. Anand SS, Singh H, Dash AK. Clinical applications of PET and PET-CT. *Med J Armed Forces India*. 2009;65(4):353-358.
3. Hicks RJ, Hofman MS. Is there still a role for SPECT–CT in oncology in the PET–CT era? *Nat Rev Clin Oncol*. 2012;9(12):712-720.
4. Maggi R. Physiology of gonadotropin-releasing hormone (GnRH): beyond the control of reproductive functions. *MOJ Anatomy & Physiology*. 2016;2(5):150-154.
5. Hierowski MT, Perla A, Redding TW, Schally AV. The presence of LHRH-like receptors in Dunning R3327H prostate tumors. *FEBS Lett*. 1983;154(1):92-96.
6. Emons G, Pahwa GS, Brack C, Sturm R, Oberheuser F, Knuppen R. Gonadotropin releasing hormone binding sites in human epithelial ovarian carcinomata. *Eur J Cancer Clin Oncol*. 1989;25(2):215-221.
7. Chien CH, Chen CH, Lee CY, Chang TC, Chen RJ, Chow SN. Detection of gonadotropin-releasing hormone receptor and its mRNA in primary human epithelial ovarian cancers. *Int J Gynecol Cancer: official journal of the International Gynecological Cancer Society*. 2004;14(3):451-458.
8. Moriya T, Suzuki T, Pilichowska M, et al. Immunohistochemical expression of gonadotropin releasing hormone receptor in human breast carcinoma. *Pathol Int*. 2001;51(5):333-337.
9. Skinner DC, Albertson AJ, Navratil A, et al. GnRH effects outside the hypothalamo-pituitary-reproductive axis. *J Neuroendocrinol*. 2009;21(4):282-292.
10. Webber KM, Perry G, Smith MA, Casadesus G. The contribution of luteinizing hormone to alzheimer disease pathogenesis. *Clin Med Res*. 2007;5(3):177-183.
11. Meethal SV, Smith MA, Bowen RL, Atwood CS. The gonadotropin connection in Alzheimer's disease. *Endocrine*. 2005;26(3):317-326.
12. Bowen RL, Smith MA, Harris PL, et al. Elevated luteinizing hormone expression colocalizes with neurons vulnerable to Alzheimer's disease pathology. *J Neurosci Res*. 2002;70(3):514-518.
13. Henderson VW, Paganini-Hill A, Emanuel CK, Dunn ME, Buckwalter JG. Estrogen replacement therapy in older women. Comparisons between Alzheimer's disease cases and nondemented control subjects. *Arch Neurol*. 1994;51(9):896-900.
14. Tang MX, Jacobs D, Stern Y, et al. Effect of oestrogen during menopause on risk and age at onset of Alzheimer's disease. *Lancet (London, England)*. 1996;348(9025):429-432.
15. Rossouw JE, Anderson GL, Prentice RL, et al. Risks and benefits of estrogen plus progestin in healthy postmenopausal women: principal results From the Women's Health Initiative randomized controlled trial. *JAMA*. 2002;288(3):321-333.
16. Wang L, Chadwick W, Park S-S, et al. Gonadotropin-releasing hormone receptor system: modulatory role in aging and neurodegeneration. *CNS Neurol Disord Drug Targets*. 2010;9(5):651-660.
17. Perrett RM, McArdle CA. Molecular mechanisms of gonadotropin-releasing hormone signaling: integrating cyclic nucleotides into the network. *Front Endocrinol*. 2013;4:1-15.
18. Fjellaksel R, Boomgaren M, Sundset R, Haraldsen IH, Hansen JH, Riss PJ. Small molecule piperazinyl-benzimidazole antagonists of the gonadotropin-releasing hormone (GnRH) receptor. *Med Chem Commun*. 2017;8(10):1965-1969.
19. Fjellaksel R, Dugalic D, Demissie TB, et al. An acylation-Finkelstein approach to radioiodination of bioactives: the role of amide group anchimeric assistance. *J Phys Org Chem*. 2018;31(7):-e3835, 1-12.
20. Fjellaksel R, Sundset R, Riss PJ, Hansen JH. Copper-mediated late-stage iodination and 123I-labelling of triazole-benzimidazole bioactives. *Synlett*. 2018;29(11):1491-1495.
21. Alavijeh MS, Palmer AM. The pivotal role of drug metabolism and pharmacokinetics in the discovery and development of new medicines. *IDrugs*. 2004;7(8):755-763.
22. Di L, Kerns EH. Application of pharmaceutical profiling assays for optimization of drug-like properties. *Curr Opin Drug Discov Devel*. 2005;8(4):495-504.
23. Pelletier JC, Chengalvala MV, Cottom JE, et al. Discovery of 6-({4-[2-(4-tert-butylphenyl)-1H-benzimidazol-4-yl]piperazin-1-

yl}methyl)quinoxal ine (WAY-207024): an orally active antagonist of the gonadotropin releasing hormone receptor (GnRH-R). *J Med Chem*. 2009;52(7):2148-2152.
24. Moldes-Anaya A, Wilkins AL, Rundberget T, Fæste CK. *In vitro* and in vivo hepatic metabolism of the fungal neurotoxin penitrem A. *Drug Chem Toxicol*. 2009;32(1):26-37.
25. Hansen T, Moe MK, Anderssen T, Strøm MB. Metabolism of small antimicrobial β2,2-amino acid derivatives by murine liver microsomes. *Eur J Drug Metab Pharmacokinet*. 2012;37(3):191-201.
26. Hermansson J, Glaumann H, Karlén B, von Bahr C. Metabolism of lidocaine in human liver *in vitro*. *Acta Pharmacol Toxicol*. 1980;47(1):49-52.
27. Swanson LW. Brain maps 4.0—Structure of the rat brain: an open access atlas with global nervous system nomenclature ontology and flatmaps. *J Comp Neurol*. 2018;526(6):935-943.
28. Jennes L, Dalati B, Conn PM. Distribution of gonadrotropin releasing hormone agonist binding sites in the rat central nervous system. *Brain Res*. 1988;452(1-2):156-164.
29. Nederpelt I, Georgi V, Schiele F, et al. Characterization of 12 GnRH peptide agonists—a kinetic perspective. *Br J Pharmacol*. 2016;173(1):128-141.

SUPPORTING INFORMATION

Additional supporting information may be found online in the Supporting Information section at the end of this article.

How to cite this article: Fjellaksel R, Moldes-Anaya A, Vasskog T, et al. Evaluation by metabolic profiling and *in vitro* autoradiography of two promising GnRH-receptor ligands for brain SPECT imaging. *J Label Compd Radiopharm*. 2020;1–13. https://doi.org/10.1002/jlcr.3820